HHS Public Access

Author manuscript

Brain Struct Funct. Author manuscript; available in PMC 2023 August 16.

Published in final edited form as:

Brain Struct Funct. 2023 May ; 228(3-4): 967–984. doi:10.1007/s00429-023-02635-w.

Preservation of KCC2 expression in axotomized abducens motoneurons and its enhancement by VEGF

Paula M. Calvo[1,2], **Rosa R. de la Cruz**[1], **Angel M. Pastor**[1], **Francisco J. Alvarez**[2]

[1]Departamento de Fisiología, Facultad de Biología, Universidad de Sevilla, 41012 Seville, Spain

[2]Department of Cell Biology, Emory University, Atlanta, GA 30322, USA

Abstract

The potassium chloride cotransporter 2 (KCC2) is the main Cl^- extruder in neurons. Any alteration in KCC2 levels leads to changes in Cl^- homeostasis and, consequently, in the polarity and amplitude of inhibitory synaptic potentials mediated by GABA or glycine. Axotomy downregulates KCC2 in many different motoneurons and it is suspected that interruption of muscle-derived factors maintaining motoneuron KCC2 expression is in part responsible. In here, we demonstrate that KCC2 is expressed in all oculomotor nuclei of cat and rat, but while trochlear and oculomotor motoneurons downregulate KCC2 after axotomy, expression is unaltered in abducens motoneurons. Exogenous application of vascular endothelial growth factor (VEGF), a neurotrophic factor expressed in muscle, upregulated KCC2 in axotomized abducens motoneurons above control levels. In parallel, a physiological study using cats chronically implanted with electrodes for recording abducens motoneurons in awake animals, demonstrated that inhibitory inputs related to off-fixations and off-directed saccades in VEGF-treated axotomized abducens motoneurons were significantly higher than in control, but eye-related excitatory signals in the on direction were unchanged. This is the first report of lack of KCC2 regulation in a motoneuron type after injury, proposing a role for VEGF in KCC2 regulation and demonstrating the link between KCC2 and synaptic inhibition in awake, behaving animals.

Keywords

Oculomotor system; Inhibitory synapses; Neurotrophic factors; Eye movements; Nerve injury

✉Francisco J. Alvarez, francisco.j.alvarez@emory.edu.

Angel M. Pastor and Francisco J. Alvarez are co-senior authors.

Author contributions The experiments were designed by FJA and AMP. Immunocytochemistry and image analysis were carried out by PMC. Electrophysiological experiments and analysis were carried out by PMC, AMP and RRC. The manuscript was written by FJA, RRC and AMP. All authors have revised and accept the final version of the manuscript.

Conflict of interest The authors have no financial or non-financial interests to disclose.

Ethical approval All animal procedures were performed at the University of Seville (Spain) and in accordance with the guidelines of the European Union (2010/63/EU) and Spanish legislation (R.D. 53/2013, BOE 34/11370-421) for the use and care of laboratory animals. They were approved by the local ethics committee (Protocol #04/11/15/349). Animal procedures also followed NIH guidelines and legislation in the US. No animal experimentation was performed in the US for this project. Work at the US (Emory University) consisted in immunocytochemical and morphological analyses of tissues collected at University of Seville in Spain. All efforts were made to reduce the number of animals used and their suffering during the present experiments and, in fact, some of the material derives from the tissue bank of previously published studies (Calvo et al. 2018, 2020).

Introduction

The K^+/Cl^- cotransporter 2 (KCC2) is the main extruder of Cl^- in neurons (Payne et al. 1996, 2003; Chamma et al. 2012; Kaila et al. 2014) and plays critical roles in Cl^- homeostasis and in maintaining the excitatory/inhibitory synaptic balance. Thus, increases in KCC2 produce inhibitory postsynaptic potentials of higher amplitude in response to the inhibitory neurotransmitters GABA or glycine. A decrease in KCC2 leads to Cl^- accumulation inside neurons, making the Cl^- equilibrium potential less negative resulting in weaker inhibition or even depolarizing postsynaptic potentials (Chamma et al. 2012; Medina et al. 2014; Côme et al. 2019). GABA depolarizing actions during early development, when KCC2 levels in neurons are low, are well known and KCC2 posterior upregulation contributes to render GABA and glycine into inhibitory neurotransmitters (Rivera et al. 1999; Zhu et al. 2008; Ben-Ari 2014; Peerboom and Wierenga 2021). In the adult, low levels of KCC2 are associated with pathologies characterized by hyperexcitability such as epilepsy, spasticity, neuropathic pain, ischemia, spinal cord injury or schizophrenia (Beverungen et al. 2020; Woo et al. 2002; Palma et al. 2006; Cramer et al. 2008; Papp et al. 2008; Boulenguez et al. 2010; Akita and Fukuda 2020; Pozzi et al. 2020), while KCC2 enhancement ameliorates dysfunction (Gagnon et al. 2013; Kahle et al. 2014; Moore et al. 2018; Lorenzo et al. 2020; Bilchak et al. 2021).

Axotomy of spinal, facial, hypoglossal and dorsal vagus motoneurons also induces rapid downregulation of *kcc2* gene expression followed by decreased KCC2 protein levels on the membrane (Nabekura et al. 2002; Toyoda et al. 2003; Tatetsu et al. 2012; Kim et al. 2018; Akhter et al. 2019). KCC2 downregulation in axotomized motoneurons causes an increase in internal Cl^- that results in GABA-induced depolarizing oscillations (Toyoda et al. 2003) resembling those found in immature neurons. Consequently, inhibitory drive is absent and GABAergic/glycinergic synapses depolarize axotomized motoneurons. When regeneration is allowed, KCC2 levels return to normal after motor axons reinnervate muscles (Tatetsu et al. 2012; Kim et al. 2018; Akhter et al. 2019), suggesting that target-derived factors are important regulators of KCC2 in motoneurons. Surprisingly, despite extensive literature linking BDNF/TrkB signaling with KCC2 regulation (Rivera et al. 2002, 2004; Aguado et al. 2003; Miletic and Miletic 2008; Boulenguez et al. 2010; Ludwig et al. 2011), axotomized motoneurons regulate KCC2 expression independent of BDNF (Akhter et al. 2019) by mechanisms currently unknown.

KCC2 regulation in axotomized extraocular motoneurons, a type of motoneuron particularly resilient to certain types of injuries, is yet unexplored. Extensive studies performed in cats chronically implanted with electrodes to monitor motoneuron function in awake unanesthetized animals have shown that axotomy of abducens motoneurons results in many physiological and synaptic changes that are responsive to a variety of trophic factors (reviewed in Benítez-Temiño et al. 2016). Recently, we found that vascular endothelial growth factor (VEGF) was the most effective neurotrophic factor in maintaining normal synaptic function on axotomized abducens motoneurons (Calvo et al. 2018, 2020). This agrees with previous research on VEGF significance for survival and maintenance of the morpho-physiological phenotype of injured motoneurons (Oosthuyse et al. 2001; Azzouz et al. 2004; Tovar-y-Romo et al. 2007). Thus, we hypothesized that (i) VEGF could be

a muscle-derived trophic factor; (ii) axotomy should downregulate KCC2 in abducens motoneurons and that (iii) exogenously supplied VEGF after axotomy prevents KCC2 downregulation.

The results surprisingly showed that axotomy did not downregulate KCC2 in abducens motoneurons. Further studies across species and in different motoneuron types demonstrated the uniqueness of this absence of regulation in abducens motoneurons. Interestingly, VEGF upregulated KCC2 in axotomized abducens motoneurons above control levels and this correlated with a potentiation of inhibition in these injured motoneurons. The results thus suggest that abducens motoneurons and VEGF are valuable models to test mechanisms that preserve KCC2 expression and inhibition in injured neurons.

Materials and methods

Animals and surgical procedures

Experiments were performed on 12 adult female cats weighing 2.0–2.5 kg obtained from an authorized supplier (Universidad de Córdoba, Spain), and 3 adult rats obtained from our animal facilities (Biology School, University of Sevilla, Spain) (Table 1 for details). Out of the 12 cats, 9 belonged to two previous studies: 7 from Calvo et al. (2018), and 2 from Calvo et al. (2020), and provided data for the abducens study. The last 3 cats were used for tibial nerve axotomy.

Abducens nerve axotomy is described in detail in Calvo et al. (2018). Briefly, the left VIth nerve was sectioned at its entry into the lateral rectus muscle and the lateral rectus muscle removed. A custom-made chamber was placed by suction in the proximal stump of the severed nerve to prevent reinnervation (i.e., the intraorbital device). VEGF was administered in axotomized animals through the proximal stump of the (left) VIth sectioned nerve (Calvo et al. 2018). Control data for testing KCC2 levels were obtained from the control side of axotomized or axotomized + VEGF-treated animals (Table 1).

For the electrophysiological analyses, the firing behavior of abducens motoneurons was recorded sequentially in two animals first in control, then after axotomy and finally after axotomy + VEGF treatment. Control recordings were also obtained from two additional animals (Calvo et al. 2018, 2020; Table 1). In all cases, animals were euthanized under deep terminal anesthesia (sodium pentobarbital, 100 mg/kg, i.p.) and transcardially perfused with physiological saline followed by fixative consisting of 4% paraformaldehyde prepared in 0.1 M sodium phosphate buffer (PB), pH 7.4. The brainstems were collected and the abducens region cut at 50 μm thickness using a vibratome.

To compare the effects of axotomy on KCC2 levels between cat abducens and spinal motoneurons three further cats were prepared for the tibial nerve axotomy. Thus, under general anesthesia (ketamine hydrochloride 20 mg/kg mixed with xylazine 0.5 mg/kg, i.m.), the left tibial nerve was sectioned, and a ligature was made to the proximal stump of the nerve to prevent regeneration. Then, the incision made in the skin was surgically sutured and the animals were allowed to recover. After 21 days the animals were perfusion-fixed as

described above and the lumbar spinal cord was extracted and cut at 50 μm thick coronal sections on a vibratome.

To test for any possible species differences, we also studied the response of KCC2 to axotomy in all extraocular motoneurons, as well as in facial motoneurons in rats. Non-extraocular cranial motoneurons have been reported to downregulate KCC2 levels after axotomy in rodents, including those of the vagus dorsal motor nucleus, and hypoglossal and facial motoneurons (Nabekura et al. 2002; Tatetsu et al. 2012; Kim et al. 2018), but no work has reported to date the effects of axotomy on KCC2 levels in the extraocular motoneurons in rats. We operated 3 adult Wistar rats. Under general anesthesia (sodium pentobarbital, 35 mg/kg, i.p.), animals were unilaterally (left side) enucleated to section the axons of all motoneurons innervating the extraocular muscles (IIIrd, IVth and VIth nerves). As muscles were also removed, this procedure prevented target reinnervation. In the same surgical session, the left facial nerve was cut and ligated to impede axonal regeneration (for more details on this procedure see Silva-Hucha et al. 2020). After 15 days, rats were transcardially perfused with physiological saline followed by 4% paraformaldehyde in PB as explained above for cats. Brainstem vibratome histological 50 μm thick sections were obtained. Control data were obtained from the unoperated side.

Immunocytochemical procedures

Free-floating sections were first washed in phosphate-buffered saline, pH 7.4 (PBS) with 0.3% TritonX-100 (PBS/TX) and then blocked with normal donkey serum (10% in PBS/TX) for 45 min prior to placing the section in primary antibody mixtures. The primary antibodies used were the following: (i) goat polyclonal antibody against choline acetyltransferase (ChAT; 1:500; Millipore, Billerica, MA, USA) for the identification of motoneurons; (ii) mouse monoclonal antibody against calretinin (1:100; Swant, Burgdorf, Switzerland), a calcium-binding protein that selectively labels the internuclear neurons of the abducens nucleus in cat (de la Cruz et al. 1998); (iii) rabbit polyclonal antibody against the rat KCC2 cotransporter (1:500; Millipore) in a region shared by KCC2a and KCC2b isoforms and thus referred as pan KCC2 (pKCC2) or simply as KCC2; (iv) rabbit polyclonal against the mouse KCC2a N-terminus (aa 20–40) (1:250; kindly provided by Dr. M.S. Airaksinen, University of Helsinki, Finland); (v) chicken polyclonal against the mouse KCC2b N-terminus (aa 8–22) (1:750; kindly provided by Dr. M.S. Airaksinen); and (vi) mouse monoclonal antibody against activating transcription factor 3 (ATF3; 1:200; Novus, CO, USA), which is expressed by axotomized neurons (Tsujino et al. 2000). Primary antibodies details, RRID numbers and specificities are shown in Table 2. Briefly, the specificities of antibodies against KCC2 and its isoforms were previously reported using KCC2a-KO or KCC2 null mutation mice (Uvarov et al. 2007; Markkanen et al. 2014). The ChAT antibody used here efficiently labels brainstem and spinal motoneurons in cats, rats and mice. The calretinin immunoreactivity shown here was used as a marker of abducens internuclear interneurons as fully characterized in a previous report (de la Cruz et al. 1998).

Secondary antibodies were all obtained from Jackson ImmunoResearch (West Baltimore Pike, West Grove, PA, USA), used at a dilution 1:100 in PBS/TX and were the following: (i) donkey anti-goat IgG coupled to FITC (for ChAT detection); (ii) donkey anti-mouse

IgG coupled to Cy5 (to label calretinin); (iii) donkey anti-rabbit IgG coupled to Cy3 (for KCC2 detection); (iv) donkey anti-rabbit IgG coupled to Cy5 (to reveal KCC2a); (v) donkey anti-chicken IgY coupled to FITC (for KCC2b visualization); and donkey anti-mouse IgG coupled to Cy5 (for ATF3 detection). Finally, sections were rinsed in PBS, mounted on glass slides and coverslipped with Vectashield mounting medium (Vector Laboratories, Burlingame, CA, USA).

Microscopy and imaging

A confocal microscope (Olympus FLUOVIEW FV1000) was used to capture image z-stacks of areas and cells of interest at X10 and X60 for panoramic and high-magnification images, respectively. Acquisition parameters were adjusted to use the maximum dynamic range of the images and kept constant to allow comparisons among neurons and animals. Confocal images were analyzed using Image J (NIH, Bethesda, MD, USA). To quantify the intensity of KCC2 immunofluorescence on the motoneuron surface, we selected focal planes at mid-nuclear level in which membrane KCC2 immunoreactivity was orthogonal to the plane of view. In each section, background measurements were taken from a 9 μm^2 square region of the neuropil in the same optical plane, next to the motoneurons and lacking any somatic or dendritic labeling. Average KCC2 immunofluorescence was measured on line profiles along the surface of the motoneurons and corrected for background level by calculating the percentage higher than background [100 × (membrane intensity average—background intensity average)/average background intensity], as previously described (Akhter et al. 2019). Because we used non-serial sections for all the analyses and the mid-cell optical section is restricted to a few confocal planes within one histological section it was impossible that the same individual motoneuron was resampled during KCC2 quantitation. In other words, our samples are independent motoneuron cross sections each belonging to a different motoneuron.

Physiological analysis

The discharge characteristics of cat abducens motoneurons have been previously described (Delgado-García et al. 1986a; Davis-López de Carrizosa et al. 2011). Abducens motoneurons display a tonic-phasic firing pattern that is proportional to eye position and velocity, respectively. The slope of the regression line between tonic firing rate and eye position during gaze holding corresponds to the neuronal eye position sensitivity (k, in spikes/s/degree). During spontaneous rapid eye movements or saccades, the slope of the regression line between firing rate and eye velocity is the neuronal eye velocity sensitivity (r, in spikes/s/degree/s). In the present study, we calculated these two parameters separately depending on the direction of eye movement with the aim of differentiating the motoneuronal signals encoded during excitatory versus inhibitory premotor drive. Thus, firing rates during eye fixations after saccades occurring in the direction of motoneuronal activation were correlated with eye position yielding the k-on parameter. On the other hand, the rate-position correlation during eye fixations following saccades in the direction of inactivation produced the k-off parameter. Similarly, r-on and r-off parameters were calculated from the rate-velocity correlation separating those saccades occurring in the direction of motoneuronal activation from those in the direction of inactivation (Delgado-García et al. 1986a, b).

Statistics

Comparisons between two groups were performed using either the Mann–Whitney rank sum test or the Student *t*-test. For comparisons between more than two groups, we used the Kruskall-Wallis one-way ANOVA test followed by Dunn's method for post hoc pairwise multiple comparisons, or either the one-way or the two-way ANOVA test followed by the post hoc Holm-Sidak method, in all cases at an overall significance level of 0.05. Statistics was carried out using SigmaPlot 11 (Systat Software, Inc., Chicago, IL, USA). When a significant difference was detected, effect sizes were measured by Cohen's *d*, that calculates differences between samples as multiples (or fractions) of the average standard deviation of the samples.

In all comparisons we pooled together motoneurons recorded in similar conditions from all animals. "*n*" therefore represents the number of motoneurons in all statistical comparisons. There are several justifications for this experimental design: (1) It reduces the number of cats used in these studies following ethical guidelines for minimizing the use of animals in research; (2) A recent thorough statistical analysis of motoneurons differences in ALS vs wildtype animals suggested that *n* = motoneurons provides a rigorous comparison, sometimes better than grouping data per animal averages, and also better describes the distribution of data points and variability in the population than animal averages which obscure possible differences among different motoneurons (Dukkipati et al. 2017); (3) *n* = motoneurons parallels common experimental designs and data analyses in electrophysiological experiments to which the anatomical data were directly compared; (4) The larger samples obtained by treating individual motoneurons as data points allow us to increase rigor when estimating effects sizes and their significance using estimating statistics by bootstrapping subsample data sets (Ho et al. 2019). We were careful to analyze similar numbers of motoneurons in each animal and to confirm lack of interanimal variability before pooling together all the data. In text, sample structures are always described as average number of motoneurons ± S.D. per animal.

We used bootstrapping according to the method of Ho et al. (2019) to estimate effect sizes and the significance of differences between control and experimental motoneurons. 5000 bootstrap samples were taken to calculate average differences and their 95% confidence intervals bias-corrected and accelerated. In this comparison *p* values report the likelihood of observing the effect size if the null hypothesis of zero difference is true. If $p < 0.05$ we interpret that the difference between means is significantly different from 0. In all cases considered significative the distribution of subsample differences display 95% CI limits that do not cross 0.

Quantitative data represented with histogram plots indicates mean ± standard error of the mean (SEM) whereas whisker box plots show the median, 25th and 75th quartiles with 90th and 10th percentile error bars. Estimated differences are represented as a Gaussian with the 95% confidence limit interval superimposed. All individual data points are graphed adjacent to summary graphs in swarm plots.

Results

KCC2 expression in abducens neurons

The abducens nucleus contains two types of neurons, motoneurons which innervate the ipsilateral lateral rectus muscle, and internuclear neurons whose axons project to contralateral medial rectus motoneurons in the oculomotor nucleus. In brainstem sections, the abducens nucleus was identified by locating motoneurons and internuclear neurons with ChAT (Fig. 1A, green-FITC) and calretinin (CR) immunolabeling, respectively (Fig. 1B, cyan-Cy5) (de la Cruz et al. 1998). The abducens nucleus showed also high pan-(p)KCC2 immunoreactivity (detecting all KCC2 isoforms) at low magnification (Fig. 1C, red-Cy3). At high magnification, the strongest pKCC2 immunoreactivity was found on the many small dendrites that traversed the abducens nucleus, while pKCC2 immunoreactivity on the surface of cell bodies was weaker.

Moreover, pKCC2 immunoreactivity on the cell bodies of ChAT-immunoreactive motoneurons (Fig. 1D) was consistently less intense than over the cell bodies of CR-immunoreactive internuclear neurons (Fig. 1E). To best quantify this difference, we set image acquisition parameters to maximize dynamic resolution of cell body immunofluorescence, although this frequently saturated dendritic labeling. A Mann–Whitney rank sum test comparing pKCC2 immunofluorescence (% higher than background) on the cell bodies of motoneurons ($n = 122$) and internuclear neurons ($n = 37$) demonstrated significantly higher levels of KCC2 in internuclear neurons ($p = 0.005$, $U = 1571$, Cohen's $d = 0.455$).

The mammalian *kcc2* gene generates two isoforms, KCC2a and KCC2b (Uvarov et al. 2007). We used isoform specific antibodies to analyze their specific cellular localization with triple immunofluorescence against ChAT, KCC2a and KCC2b in both the abducens nucleus and the spinal cord motoneurons. Immunolabeling with KCC2b was similar in appearance to that with pKCC2, both strongly expressed on the surface of dendrites and clearly delineating the somatic plasma membrane of motoneurons (Fig. 1F–G). In contrast, KCC2a immunolabeling yielded mostly intracellular labeling in soma and dendrites of ChAT-positive motoneurons (Fig. 1H–I). Similar results were obtained in the spinal cord.

Axotomy does not modify KCC2 levels in cat abducens motoneurons and VEGF induces an upregulation

We expected that, in accordance with other cranial and spinal motoneurons, abducens motoneurons would downregulate KCC2 expression following axotomy and we hypothesized KCC2 downregulation could be prevented with VEGF, because this neurotrophic factor fully recovers the discharge alterations induced by axotomy in abducens motoneurons (Calvo et al. 2018, 2020). Double immunofluorescence was carried out for ChAT and pKCC2 in control and axotomized motoneurons treated or not with VEGF (Fig. 2A–I). For these analyses we pooled all motoneurons sampled from 6 control abducens ($n = 122$ motoneurons; 20.3 ± 3.9 average per animal ± S.D.), 3 axotomized ($n = 71$ motoneurons; 23.7 ± 3.8) and 3 axotomized treated with VEGF ($n = 72$ motoneurons; 24.0 ± 2.9). After the interval of 3 weeks post-lesion surprisingly pKCC2 immunolabeling

surrounding injured abducens motoneurons was unchanged compared to control (Fig. 2A–C vs. D–F). In contrast, motoneurons treated with VEGF showed higher levels (Fig. 2G–I). Abducens internuclear neurons (ChAT-negative, marked by an asterisk in Fig. 2D–I) displayed their normal high levels of pKCC2 in all conditions. A one-way ANOVA test revealed the existence of significant differences on pKCC2 immunofluorescence among axotomized motoneurons treated with VEGF, untreated axotomized and control motoneurons (Fig. 2J; $F_{(2, 262)} = 4.671$, $p = 0.01$, $d = 0.486$). Pairwise multiple comparisons (Holm-Sidak method) demonstrated that there was no difference between control and axotomy ($p = 0.394$), whereas axotomized + VEGF-treated motoneurons showed significantly higher pKCC2 immunofluorescence than both control ($p = 0.017$) and axotomy ($p = 0.004$). In summary, axotomy did not downregulate KCC2 in abducens motoneurons but VEGF increased significantly the level of membrane KCC2 detected with immunofluorescence.

To further define the increase in pKCC2 we used estimation statistics (Fig. 2K). For this purpose, 5000 bootstrap data set were obtained to perform aleatory comparisons between subsample pairs and estimate an average difference and 95% confidence intervals (CI) for the size of possible differences and their significance using a two-sided permutation *t*-test. Comparisons between control ($n = 122$) and axotomized motoneurons ($n = 71$) indicated that the 95% CI of average differences between axotomized motoneurons and controls ranged from a 22% decrease to an 8% increase with $p = 0.366$ (2-sided permutation *t*-test) suggesting lack of significance. However, when comparing control motoneurons to VEGF-treated animals the 95% CI for their differences ranged between 4 and 40% increases with $p = 0.026$ (2-sided permutation *t*-test) and the average estimated difference suggested a 21% increase in KCC2 immunofluorescence pixel density surrounding the cell body compared to control and 22% increase when compared to non-VEGF-treated axotomized motoneurons. This effect correlated with a functional enhancement of inhibition, as shown below.

Preservation of KCC2 in axotomized cat abducens motoneurons is not a species-specific phenomenon

The lack of KCC2 change in axotomized cat abducens motoneurons contrasted markedly with the strong downregulation known to occur in spinal and other brainstem motoneurons following their axotomy in rodents (Nabekura et al. 2002; Tatetsu et al. 2012; Kim et al. 2018; Akhter et al. 2019). To discard the possibility that cat motoneurons in general lack KCC2 regulation after axotomy, we analyzed axotomized spinal motoneurons in the cat. For this purpose, the tibial nerve was cut in three cats and a ligature made in the proximal stump of the nerve to prevent regeneration. Twenty-one days later, tissue from these animals was processed for triple immunofluorescence ChAT, pKCC2 and ATF3. Control spinal motoneurons were identified in the contralateral side by ChAT (Fig. 3A), they displayed pKCC2 on the somatic membrane (Fig. 3B), and lacked ATF3 nuclear labeling (Fig. 3C) ($n = 96$ control motoneurons; 32.0 ± 2.9 per animal). ChAT and ATF3 were used to positively identify axotomized spinal motoneurons (Fig. 3E–G) ($n = 101$ axotomized motoneurons; 33.7 ± 1.7 per animal). They lacked pKCC2 on their membrane (Fig. 3F). Figures 3D, H illustrate the merge of the triple immunofluorescence in a control and an axotomized motoneuron, respectively. In contrast to cat abducens motoneurons, axotomized

ATF3-positive spinal cat motoneurons significantly downregulated pKCC2 (Fig. 3L; *t*-test, $p \leq 0.001$, $t_{(195)} = 20.142$). Estimation of effect size differences suggested this was close to 3 standard deviations ($d = 2.871$) with a 95% CI ranging from a 63 to 77% decreases in pKCC2 pixel density, averaging a 70% decrease that was highly significant ($p < 0.0001$, 2-sided permutation test) (Fig. 2M). These findings suggest that spinal motoneurons in the cat downregulate KCC2 normally after axotomy and that the absence of change in abducens motoneurons is not a general response of cat motoneurons, but specific to the abducens nucleus.

KCC2b is the preferential isoform present and regulated on the motoneuron cell body

KCC2b and pKCC2 showed similar distributions on the somatic membrane of abducens and spinal motoneurons. Thus, we compared whether both are co-regulated after axotomy in spinal and abducens motoneurons. Comparisons between both immunostainings were done in control and axotomized motoneurons obtained from one cat in the abducens nucleus (Fig. 1F–G and 2N) and one cat in the spinal cord (Fig. 3I–K and N). Two-way ANOVA for KCC2 immunoreactivity (pKCC2 or KCC2b), experimental condition (control or axotomized) and any possible interaction (Fig. 2K) found no significant differences in abducens motoneurons (pKCC2 vs KCC2b, $p = 0.089$, $F_{(1,108)} = 2.937$; control vs. axotomized, $p = 0.166$, $F_{(1,108)} = 1.946$; interaction, $p = 0.207$, $F_{(1,108)} = 1.611$; $n = 27$ and 24 control and $n = 29$ and 32 axotomized motoneurons analyzed for pKCC2 and KCC2b respectively in each experimental situation). In the spinal cord a similar two-way ANOVA (Fig. 3M) detected a significant reduction in control vs. axotomized motoneurons ($p < 0.001$, $F_{(1,111)} = 207.044$; $n = 29$ and 26 control and $n = 33$ and 27 axotomized motoneurons for respectively pKCC2 and KCC2b; Cohen's $d = -2.8$ for pKCC2 and -2.6 for KCC2b), but there was no difference between pKCC2 and KCC2b (they changed in parallel) ($p = 0.099$, $F_{(1,111)} = 2.763$) or the interaction between axotomy and type of immunoreactivity ($p = 0.334$, $F_{(1,111)} = 0.942$). *Post hoc* Holm-Sidak methods revealed significant difference between control and injured motoneuron for pKCC2 and KCC2b ($p < 0.001$ for both). However, no significant differences in somatic membrane immunofluorescence were found between pKCC2 and KCC2b in control ($p = 0.071$) or axotomy ($p = 0.619$).

To further support similar regulation of pKCC2 and KCC2b in spinal motoneurons we compared the effect of axotomy on the decrease of each immunofluorescence in a single animal in which pKCC2 and KCC2b were compared in parallel. We found that the 95% CI of the difference to control suggested a decrease in pKCC2 ranging from 60 to 85% with an average of 72% decrease with respect to control value and this was highly significant ($p < 0.0001$, 2-sided permutation test). KCC2b depletions paralleled the decrease in pKCC2 with a 95% CI decrease ranging from 59 to 88%, averaging a highly significant 72% decrease ($p < 0.0001$, 2-sided permutation *t*-test) (Fig. 3O). KCC2b is therefore the isoform principally expressed and regulated on the somatic plasma membrane of abducens and spinal motoneurons and pKCC2 and KCC2b immunoreactivities are interchangeable in this model.

Abducens motoneurons are unique across species in their preservation of KCC2 among brainstem motoneurons

Next, we analyzed whether the absence of change in KCC2 after axotomy in abducens motoneurons was unique to the cat by comparing KCC2 regulation after axotomy in the rat abducens nucleus. We compared KCC2 regulation after axotomy in the motoneurons of the three oculomotor nuclei (abducens, trochlear and oculomotor) as well as in other cranial motoneurons (facial nucleus). For this purpose, three adult rats were enucleated unilaterally (left side), a procedure that axotomizes all extraocular motoneurons and leave them target deprived. In the same surgical session, the left facial nerve was also sectioned as a reference, since it is well-established that axotomized facial motoneurons in the rat downregulate KCC2 expression (Toyoda et al. 2003). KCC2 levels were evaluated 15 days post-lesion in the four brainstem nuclei by means of triple immunofluorescence against ChAT, pKCC2, and ATF3 and compared to control motoneurons in the contralateral side. pKCC2 immunofluorescence was markedly decreased in axotomized oculomotor (Fig. 4A–B; the white arrow points to nuclear ATF3 staining, as a marker of neuronal injury), trochlear (Fig. 4C–D) and facial (Fig. 4G–H) motoneurons. In contrast -as happened in the cat–rat abducens motoneurons displayed similar pKCC2 in axotomy and control. In addition, and in parallel with the cat, ATF3 did not label rat axotomized abducens motoneurons (Fig. 4E–F). Quantification of pKCC2 immunofluorescence in all nuclei was compared using a two-way ANOVA test (two factors: nucleus and treatment) followed by Holm-Sidak method for pairwise comparisons (Fig. 4I). Axotomized oculomotor, trochlear and facial motoneurons had significantly lower KCC2 immunofluorescence than their respective controls (Fig. 4I, asterisks; $p < 0.001$ for the three motoneuronal types). No significant differences were found between axotomized and control abducens motoneurons ($p = 0.564$). The three oculomotor nuclei exhibited a similar value of pKCC2 immunofluorescence in the control situation (abducens vs. oculomotor $p = 0.128$; abducens vs. trochlear $p = 0.081$; oculomotor vs. trochlear $p = 0.827$), while the facial nuclei had slightly higher pKCC2 immuno-reactivity compared to oculomotor ($p = 0.021$) and trochlear ($p = 0.011$), but not when compared against abducens ($p = 0.445$). Axotomized motoneurons drastically downregulated KCC2 immunofluorescence to similar low levels in oculomotor, trochlear and facial, but not in the abducens. As a result, axotomized abducens motoneurons showed a significantly higher value of pKCC2 labeling than the other three motoneuronal types after axotomy (Fig. 4I, hashtag; $p < 0.001$ for all cases; $n = 35$, 36, 33 and 39 motoneurons for control and $n = 33$, 35, 44 and 42 for axotomized motoneurons of the oculomotor, trochlear, abducens and facial nuclei, respectively, Cohens' $d = -1.9$ for oculomotor, -3.0 fr trochlear and -2.9 for facial). Estimated differences after creating bootstrapped datasets ranged from 57 to 100% depletions from control with average reductions of 72%, 89% and 87% membrane pKCC2 immunoreactivity, respectively for oculomotor, trochlear and facial motoneurons, and in all cases this being highly significant ($p < 0.001$, 2-side permutation t-test). This was not the case for abducens axotomized motoneurons which showed no significant effect in pKCC2 immunoreactivity compared to controls ($p = 0.655$; 2-sided permutation t-test; average estimated difference < 5% from control, with a broad range in different bootstrapped data sets ranging in 95% CI from 15% depletion to a 24% increase).

In conclusion, preservation of KCC2 in axotomized abducens motoneurons was similar in cats and rats. Since nerve injury in our rat surgical model occurs simultaneously and by the same procedure (eye enucleation) in all three groups of extraocular motoneurons, we can exclude the possibility of differential levels of injury, and conclude that the response to axotomy of abducens motoneurons is unique to them across species and not a general feature of extraocular motoneuronal nuclei.

Discharge signals derived from inhibitory synapses increase by VEGF in axotomized abducens motoneurons

Control abducens motoneurons have a tonic-phasic firing pattern that correlates with eye position and velocity (Delgado-García et al. 1986a; Davis-López de Carrizosa et al. 2011). These motoneurons discharge monotonically at higher frequencies for gaze fixations set at more eccentric eye positions in the direction of activation (on-direction) and decrease their firing rate for those fixations in the off-direction (Fig. 5A). Therefore, there is a correlation between firing rate and eye position in control motoneurons (Fig. 5B). The slope of this regression line is named k (in spikes/s/degree; black line in Fig. 5B). The tonic component of the discharge can be analyzed differentiating between those fixations occurring after an on-directed saccade (arrows in Fig. 5A) versus those occurring after an off-directed saccade (arrowheads in Fig. 5A). This led to two distinct rate-position correlations, after separating those fixations following on-saccades from those attained after off-saccades. Therefore, two regression lines were obtained whose slopes were k-on (orange line and dots in Fig. 5B) and k-off (red line and dots in Fig. 5b), being k-on related to modulation of excitatory inputs (increases in firing) and k-off related to modulation of inhibitory inputs (decreases in firing).

Control abducens motoneurons also exhibit a phasic component, displayed in the form of a high-frequency burst of spikes for those saccades in the on-direction (arrows in Fig. 5C) and an abrupt decay in firing rate or a pause for off-directed saccades (arrowheads in Fig. 5C). Those off-saccades resulting from a cease in motoneuronal discharge (asterisks in Fig. 5C) were not considered for the analysis. The correlation between firing rate (previous subtraction of the eye position component) and eye velocity during saccades fits to a regression line whose slope is the neuronal eye velocity sensitivity (r, in spikes/s/degree/s; black line in Fig. 5D). When the rate-velocity correlation was performed separating on- versus off-saccades, then the parameters r-on (orange line and dots in Fig. 5D) and r-off (red line and dots in Fig. 5D) were obtained (for more details see Delgado-García et al. 1986a, b). k-on and r-on represent the excitatory drive in abducens motoneurons arising from specific excitatory inputs, whereas k-off and r-off are the result of the inhibitory drive originating from inhibitory inputs to the abducens nucleus (Escudero and Delgado-García 1988; Escudero et al. 1992).

We compared the excitatory signals, k-on and r-on, and the inhibitory signals, k-off and r-off, in abducens motoneurons under the different situations (control, axotomy, axotomy + VEGF) to determine whether there was a correlation between KCC2 level and inhibitory synaptic drive. Neurophysiological recordings were re-analyzed from our previous work (Calvo et al. 2018) (control, $n = 21$; axotomy, $n = 17$; axotomy + VEGF, $n = 18$). Significant differences were detected among the three groups for k-off (Kruskal–Wallis

one-way ANOVA test, $p \leq 0.001$, $H = 23.625$, $d = 1.66$) and r-off (Kruskal–Wallis one-way ANOVA test, $p \leq 0.001$, $H = 19.441$, $d = 1.401$). Dunn's pairwise multiple comparisons showed higher k-off and r-off in abducens axotomized motoneurons treated with VEGF compared with untreated control and axotomized motoneurons (asterisks in Fig. 6A–B; $p < 0.05$ for k-off as well as r-off), whereas there was no significant difference in k-off and r-off between control and axotomized abducens motoneurons ($p > 0.05$).

On the other hand, axotomized abducens motoneurons treated with VEGF had similar k-on and r-on values compared to control ($p > 0.05$ for both; $Q = 0.668$ for k-on and $Q = 1.514$ for r-on, Dunn's pairwise comparisons), whereas axotomized motoneurons presented significantly lower k-on ($p < 0.05$, $Q = 3.379$) and r-on than control ($p < 0.05$, $Q = 2.876$) and or axotomized VEGF-treated motoneurons ($p < 0.05$ for both, $Q = 3.894$ for k-on and $Q = 4.212$ for r-on) (Fig. 6C–D). For comparisons between the three groups, Kruskal–Wallis one-way ANOVA test was used ($p \leq 0.001$, $H = 17.540$, $d = 1.288$, for k-on; $p < 0.001$, $H = 18.326$, $d = 1.334$, for r-on), followed by Dunn's method for all pairwise multiple comparisons.

Therefore, inhibition increase (larger k-off and r-off) in axotomized motoneurons treated with VEGF correlated with the findings of higher levels of KCC2 immunofluorescence in axotomized + VEGF-treated abducens motoneurons, which likely led to larger Cl^- extrusion and a more hyperpolarized E_{Cl^-}, which strengthens inhibitory synaptic transmission.

Discussion

The present results show that axotomy did not modify KCC2 in abducens motoneurons of cats and rats, in contrast to the downregulation in other brainstem and spinal motoneurons after axotomy in both species. This suggests that abducens motoneurons are unique in the lack of KCC2 regulation after axotomy. Our findings also indicated that the expression and changes in KCC2 at the soma surface of motoneurons were due mainly to the KCC2b isoform. Finally, administration of VEGF to axotomized abducens motoneurons significantly upregulated the levels of KCC2 above control and axotomy, and this correlated with an increase in off-related discharges of abducens motoneurons recorded in alert cats. Previous studies highlighted BDNF as an important regulator of KCC2 expression during development and after injuries or neuropathology in adults (Lee-Hotta et al. 2019). Our results suggest, however, that in motoneurons, VEGF regulates KCC2 expression. Since VEGF is produced by muscle, and KCC2 expression in motoneurons depend on muscle innervation (Akhter et al. 2019), it is possible that VEGF could act as a target-derived neurotrophic factor (Calvo et al. 2018, 2020) modulating KCC2 expression in motoneurons.

Differential regulation of KCC2 in abducens and spinal motoneurons after axotomy

The most striking result was that abducens motoneurons did not downregulate KCC2 after axotomy despite using a method extensively validated for chronic axotomy of abducens motoneurons in the cat (David López de Carrizosa et al. 2008, 2009, 2010; Calvo et al. 2018, 2020). The absence of change was not generalizable to all extraocular motoneurons, since oculomotor and trochlear motoneurons downregulated KCC2 after axotomy, similar to other spinal and brainstem motoneurons studied to date in rodents (Nabekura et al.

2002; Toyoda et al. 2003; Tatetsu et al. 2012; Kim et al. 2018; Akhter et al. 2019). A cat-specific response does not explain KCC2 preservation either, since axotomized spinal motoneurons in the cat showed normal KCC2 downregulation after axotomy, and rat abducens motoneurons did not downregulate KCC2, similar to the cat. In parallel, ATF3 was not expressed by axotomized abducens motoneurons. ATF3 upregulation is a consistent phenomenon in all previously studied motoneurons and sensory neurons after axotomy (Tsujino et al. 2000; Holland et al. 2019) and is part of signaling cascades leading to coordinated stress and/or regeneration responses in neurons (Patodia and Raivich 2012). However, although ATF3 enhances regeneration, alone does not entirely recapitulate the whole regenerative program (Seijffers et al. 2007), and its deletion does not fully prevent axon regeneration (Gey et al. 2016; Holland et al. 2019). This suggests the possibility of a multiplexed response to injury that might not be identical for every motoneuron. It is possible that abducens motoneurons are at one extreme of a diversity of motoneuronal responses to injury and regeneration, being in this case ATF3-independent and preserving KCC2 expression. Whether there is a causal link between ATF3 upregulation and KCC2 downregulation needs to be further studied. Nonetheless, many other properties of axotomized motoneurons are present in abducens motoneurons; these include changes in physiological properties, synaptic plasticity and neighboring glial reactions (Delgado-García et al. 1988; Davis-López de Carrizosa et al. 2009, 2010). The possible implications for neuroprotection and regeneration, that may be unique to abducens motoneuron responses to injury are interesting avenues for future enquiry raised by the present results.

VEGF upregulates KCC2 levels in axotomized abducens motoneurons

Although VEGF was initially discovered by its action on blood vessels, from an evolutionary point of view it emerged earlier as a neurotrophic factor, since it is essential for the development of the nervous system in invertebrates lacking a vascular system or having a rudimentary vasculature (Zacchigna et al. 2008). Nowadays, it is accepted that VEGF is neuroprotective (Silva-Hucha et al. 2020). Our results show that exogenous VEGF upregulated KCC2 in axotomized abducens motoneurons, and that this correlated with increased efficiency of inhibitory signals in these motoneurons. To our knowledge, this is the first time that KCC2 expression has been related to VEGF, however, the related KCC3 was shown regulated by VEGF during its initial characterization (Hiki et al. 1999).

KCC2 transcription is promoted by Egr transcriptional factors downstream of the rat sarcoma MAP kinase (Ras/MAPK) pathway (Ludwig et al. 2011) and several neurotrophic factors converge in this pathway, including BDNF-TrkB and VEGF-VEGFR2. KCC2 transcriptional regulation by BDNF has been found to be context dependent. Thus, during development BDNF upregulates KCC2 and is involved in the switch of depolarizing to hyperpolarizing actions of GABA (Aguado et al. 2003; Ludwig et al. 2011). On the other hand, increases in local BDNF after injury in the adult frequently downregulate KCC2 in many neurons (Rivera et al. 2002, 2004; Miletic and Miletic 2008; Boulenguez et al. 2010), and effects are dependent on the signaling pathway selected downstream of TrkB (Rivera et al. 2004). In adult neurons, KCC2 transcription is downregulated by PLCγ1 or Shc/FRS-2 signaling and upregulated by PI3K and Ras/MAPK (Rivera et al. 2004). VEGF-VEGFR2

strongly activates PI3K and Ras/MAPK cascades, while having limited effects on PLCγ1 or Shc/FRS-2 pathways.

In addition to transcriptional regulation, posttranslational dephosphorylation at specific KCC2 residues causes internalization (Lee et al. 2011; Bos et al. 2013). BDNF activation of Shc/FRS-2 results in degradation of internalized KCC2 reducing membrane levels. We previously showed that KCC2 removal from axotomized spinal motoneurons is secondary to reduced *kcc2* mRNA expression independent of BDNF/TrkB, and KCC2 recovery occurred only after motoneurons reinnervated muscle (Akhter et al. 2019). Likewise, muscle reinnervation restores KCC2 in axotomized facial (Kim et al. 2018) and hypoglossal motoneurons (Tatetsu et al. 2012). Muscles express VEGF, where it mediates hypoxia-induced angiogenesis during exercise and physiological adaptations (Gustafsson 2011; Hoier and Hellsten 2014). VEGF is expressed in the lateral rectus muscle, and abducens motoneurons and their axons in the muscle are endowed with VEGF receptors (Calvo et al. 2018; Silva-Hucha et al. 2020). It is thus possible that target-derived VEGF acts as a retrograde factor regulating KCC2 in motoneurons. Axotomy did not downregulate KCC2 in abducens motoneurons however, suggesting that additional factors are necessary or that abducens motoneurons obtain VEGF from alternative sources when disconnected from muscle. Nevertheless, exogenous application of VEGF upregulated KCC2 expression above normal levels in injured abducens motoneurons.

Functional correlates of VEGF upregulation of KCC2 in axotomized abducens motoneurons

VEGF was shown to maintain normal physiological properties in axotomized motoneurons with higher efficiency than other trophic factors (Calvo et al. 2018, 2020). Axotomy changes abducens motoneuron firing because it alters both intrinsic properties and function of synaptic inputs (Delgado-García et al. 1988; Calvo et al. 2018, 2020). BDNF and NT-3 recover responses of axotomized abducens motoneurons to, respectively, tonic and phasic inputs (Davis-López de Carrizosa et al. 2009), and NGF recovers most properties and synaptic inputs, but above control values and with high variability. Only VEGF consistently recovers all axotomy-induced alterations to control levels (Calvo et al. 2018, 2020). In here, we re-analyzed our recordings to extract specifically the gains of inhibitory off-rates and found a specific enhancement of inhibitory inputs (i.e., k-off and r-off) by VEGF that was not previously reported.

VEGF restores to control values overall eye position and eye velocity sensitivities (i.e., k and r) in axotomized motoneurons (Calvo et al. 2018). Herein, both sensitivities were calculated separately during on versus off fixations (i.e., k-on and k-off) as well as for on-directed versus off-directed saccades (i.e., r-on and r-off), being on the direction of the lateral rectus muscle contraction and off the direction of relaxation. Axotomized abducens motoneurons treated with VEGF exhibited higher k-off and r-off than control motoneurons. In contrast, k-on and r-on were similar to control. This implied that VEGF increased inhibitory synaptic input strength, in agreement with KCC2 upregulation. This conclusion might also explain previous results on internuclear abducens neurons axotomized at the level of medial longitudinal fascicle. This manipulation also decreases excitatory and inhibitory

inputs in these neurons, but when cut axons are provided with an implant of neural progenitor cells, they retain inhibitory synapses and off-signals similar to control values, whereas excitatory drive decreases normally (Morado-Díaz et al. 2014). Neural progenitor cells express VEGF and it was suggested that this neurotrophic factor could exert a direct influence in the efficacy of inhibitory signals (Talaverón et al. 2013; Morado-Díaz et al. 2014). The data presented here confirm that VEGF treatment upregulates KCC2 and can maintain or enhance inhibition in injured neurons.

The causal link between VEGF and the upregulation of KCC2 opens the possibility that the ionic balance is preserved when neurons access a source of trophic factors that keep KCC2 expression at mature levels in motoneurons. The maintenance of inhibitory chloride currents might also protect motoneurons from the deleterious action of calcium-dependent excitotoxicity that makes motoneurons vulnerable in certain pathologies such as amyotrophic lateral sclerosis (Fuchs et al. 2010).

Funding

This work was funded by NIH (NINDS) R01 NS111969 and R21 NS114839 to F.J.A. This publication is also part of the I + D + i project P20_00529 Consejería de Transformatión Económica Industria y Conocimiento, Junta de Andalucía-FEDER. Research materials were also supported by project PGC2018-094654-B-100 and PID2021-124300NB-I00 both funded by MCIN/AEI/FEDER “A way of making Europe” to A.M.P and RRC. P.M.C. was a scholar of Ministerio de Educatión y Ciencia (BES-2016–077912) in Spain and now a “Margarita Salas” postdoctoral fellow from Spain at Emory University Atlanta, USA.

Data availability

The data supporting this study are available upon reasonable request to the authors.

References

Aguado F, Carmona MA, Pozas E, Aguiló A, Martínez-Guijarro FJ, Alcantara S, Borrell V, Yuste R, Ibañez CF, Soriano E (2003) BDNF regulates spontaneous correlated activity at early developmental stages by increasing synaptogenesis and expression of the K+/Cl− co-transporter KCC2. Development 130:1267–1280. 10.1242/dev.00351 [PubMed: 12588844]

Akhter ET, Griffith RW, English AW, Alvarez FJ (2019) Removal of the potassium chloride co-transporter from the somatodendritic membrane of axotomized motoneurons is independent of BDNF/TrkB signaling but is controlled by neuromuscular innervation. eNeuro 6:5. 10.1523/eneuro.0172-19.2019

Akita T, Fukuda A (2020) Intracellular Cl^- dysregulation causing and caused by pathogenic neuronal activity. Pflugers Arch 472:977–987. 10.1007/s00424-020-02375-4 [PubMed: 32300887]

Azzouz M, Ralph GS, Storkebaum E, Walmsley LE, Mitrophanous KA, Kingsman SM, Carmeliet P, Mazarakis ND (2004) VEGF delivery with retrogradely transported lentivector prolongs survival in a mouse ALS model. Nature 429:413–417. 10.1038/nature02544 [PubMed: 15164063]

Ben-Ari Y (2014) The GABA excitatory/inhibitory developmental sequence: a personal journey. Neuroscience 279:187–219. 10.1016/j.neuroscience.2014.08.001 [PubMed: 25168736]

Benítez-Temiño B, Davis-López de Carrizosa MA, Morcuende S, Matarredona ER, de la Cruz RR, Pastor AM (2016) Functional diversity of neurotrophin actions on the oculomotor system. Int J Mol Sci 17:2016. 10.3390/ijms17122016 [PubMed: 27916956]

Beverungen H, Klaszky SC, Klaszky M, Côté MP (2020) Rehabilitation decreases spasticity by restoring chloride homeostasis through the brain-derived neurotrophic factor-KCC2 pathway after spinal cord injury. J Neurotrauma 37:846–859. 10.1089/neu.2019.6526 [PubMed: 31578924]

Bilchak JN, Yeakle K, Caron G, Malloy D, Côté MP (2021) Enhancing KCC2 activity decreases hyperreflexia and spasticity after chronic spinal cord injury. Exp Neurol 338:113605. 10.1016/j.expneurol.2021.113605 [PubMed: 33453210]

Bos R, Sadlaoud K, Boulenguez P, Buttigieg D, Liabeuf S, Brocard C, Haase G, Bras H, Vinay L (2013) Activation of 5-HT2A receptors upregulates the function of the neuronal K-Cl cotransporter KCC2. Proc Natl Acad Sci USA 110:348–353. 10.1073/pnas.1213680110 [PubMed: 23248270]

Boulenguez P, Liabeuf S, Bos R, Bras H, Jean-Xavier C, Cécile Brocard C, Stil A, Darbon P, Cattaert D, Delpire E, Marsala M, Vinay L (2010) Down-regulation of the potassium-chloride cotransporter KCC2 contributes to spasticity after spinal cord injury. Nat Med 16:302–307. 10.1038/nm.2107 [PubMed: 20190766]

Calvo PM, de la Cruz RR, Pastor AM (2018) Synaptic loss and firing alterations in axotomized motoneurons are restored by vascular endothelial growth factor (VEGF) and VEGF-B. Exp Neurol 304:67–81. 10.1016/j.expneurol.2018.03.004 [PubMed: 29522757]

Calvo PM, de la Cruz RR, Pastor AM (2020) A single intraventricular injection of VEGF leads to long-term neurotrophic effects in axotomized motoneurons. eNeuro 7:3. 10.1523/eneuro.0467-19.2020

Chamma I, Chevy Q, Poncer JC, Lévi S (2012) Role of the neuronal K-Cl co-transporter KCC2 in inhibitory and excitatory neurotransmission. Front Cell Neurosci 6:5. 10.3389/fncel.2012.00005 [PubMed: 22363264]

Côme E, Heubl M, Schwartz EJ, Poncer JC, Lévi S (2019) Reciprocal regulation of KCC2 trafficking and synaptic activity. Front Cell Neurosci 13:48. 10.3389/fncel.2019.00048 [PubMed: 30842727]

Cramer SW, Baggott C, Cain J, Tilghman J, Allcock B, Miranpuri G, Rajpal S, Sun D, Resnick D (2008) The role of cation-dependent chloride transporters in neuropathic pain following spinal cord injury. Mol Pain 4:36. 10.1186/1744-8069-4-36 [PubMed: 18799000]

Davis-López de Carrizosa MA, Tena JJ, Benítez-Temiño B, Morado-Díaz CJ, Pastor AM, de la Cruz RR (2008) A chronically implantable device for the controlled delivery of substances, and stimulation and recording of activity in severed nerves. J Neurosci Methods 167:302–309. 10.1016/j.jneumeth.2007.08.021 [PubMed: 17935791]

Davis-López de Carrizosa MA, Morado-Díaz CJ, Tena JJ, Benítez-Temiño B, Pecero ML, Morcuende SR, de la Cruz RR, Pastor AM (2009) Complementary actions of BDNF and neurotrophin-3 on the firing patterns and synaptic composition of motoneurons. J Neurosci 29:575–587. 10.1523/jneurosci.5312-08.2009 [PubMed: 19144857]

Davis-López de Carrizosa MA, Morado-Díaz CJ, Morcuende S, de la Cruz RR, Pastor AM (2010) Nerve growth factor regulates the firing patterns and synaptic composition of motoneurons. J Neurosci 30:8308–8319. 10.1523/jneurosci.0719-10.2010 [PubMed: 20554882]

Davis-López de Carrizosa MA, Morado-Díaz CJ, Miller JM, de la Cruz RR, Pastor AM (2011) Dual encoding of muscle tension and eye position by abducens motoneurons. J Neurosci 31:2271–2279. 10.1523/jneurosci.5416-10.2011 [PubMed: 21307263]

de la Cruz RR, Pastor AM, Martínez-Guijarro FJ, López-García C, Delgado-García JM (1998) Localization of parvalbumin, calretinin, and calbindin D-28k in identified extraocular motoneurons and internuclear neurons of the cat. J Comp Neurol 390:377–391. 10.1002/(sici)1096-9861(19980119)390:3<377::aid-cne6>3.0.co;2-z [PubMed: 9455899]

Delgado-García JM, del Pozo F, Baker R (1986a) Behavior of neurons in the abducens nucleus of the alert cat-I. Motoneurons Neuroscience 17:929–952. 10.1016/0306-4522(86)90072-2 [PubMed: 3487043]

Delgado-García JM, del Pozo F, Baker R (1986b) Behavior of neurons in the abducens nucleus of the alert cat-II. Internuclear Neurons Neuroscience 17:953–973. 10.1016/0306-4522(86)90073-4 [PubMed: 3487044]

Delgado-García JM, Del Pozo F, Spencer RF, Baker R (1988) Behavior of neurons in the abducens nucleus of the alert cat-III. Axotomized Motoneurons Neurosci 24:143–160. 10.1016/0306-4522(88)90319-3

Dukkipati SS, Chihi A, Wang Y, Elbasiouny SM (2017) Experimental design and data analysis issues contribute to inconsistent results of C-bouton changes in amyotrophic lateral sclerosis. eNeuro 4(1):ENEURO.0281-16.2016. 10.1523/ENEURO.0281-16.2016

Escudero M, Delgado-García JM (1988) Behavior of reticular, vestibular and prepositus neurons terminating in the abducens nucleus of the alert cat. Exp Brain Res 71:218–222. 10.1007/bf00247538 [PubMed: 3416954]

Escudero M, de la Cruz RR, Delgado-García JM (1992) A physiological study of vestibular and prepositus hypoglossi neurones projecting to the abducens nucleus in the alert cat. J Physiol 458:539–560. 10.1113/jphysiol.1992.sp019433 [PubMed: 1302278]

Fuchs A, Ringer C, Bilkei-Gorzo A, Weihe E, Roeper J, Schütz B (2010) Downregulation of the potassium chloride cotransporter KCC2 in vulnerable motoneurons in the SOD1-G93A mouse model of amyotrophic lateral sclerosis. J Neuropathol Exp Neurol 10:1057–1070. 10.1097/nen.0b013e3181f4dcef

Gagnon M, Bergeron MJ, Lavertu G, Castonguay A, Tripathy S, Bonin RP, Perez-Sanchez J, Boudreau D, Wang B, Dumas L, Valade I, Bachand K, Jacob-Wagner M, Tardif C, Kianicka I, Isenring P, Attardo G, Coull JA, De Koninck Y (2013) Chloride extrusion enhancers as novel therapeutics for neurological diseases. Nat Med 19:1524–1528. 10.1038/nm.3356 [PubMed: 24097188]

Gey M, Wanner R, Schilling C, Pedro MT, Sinske D, Knöll B (2016) Atf3 mutant mice show reduced axon regeneration and impaired regeneration-associated gene induction after peripheral nerve injury. Open Biol 6:160091. 10.1098/rsob.160091 [PubMed: 27581653]

Gustafsson T (2011) Vascular remodelling in human skeletal muscle. Biochem Soc Trans 39:1628–1632. 10.1042/bst20110720 [PubMed: 22103498]

Hiki K, D'Andrea RJ, Furze J, Crawford J, Woollatt E, Sutherland GR, Vadas MA, Gamble JR (1999) Cloning, characterization, and chromosomal location of a novel human K+-Cl− cotransporter. J Biol Chem 274:10661–106617 [PubMed: 10187864]

Ho J, Tumkaya T, Aryal S, Choi H, Claridge-Chang A (2019) Moving beyond P values: data analysis with estimation graphics. Nat Methods 16:565–566. 10.1038/s41592-019-0470-3 [PubMed: 31217592]

Hoier B, Hellsten Y (2014) Exercise-induced capillary growth in human skeletal muscle and the dynamics of VEGF. Microcirculation 21:301–314. 10.1074/jbc.274.15.10661 [PubMed: 24450403]

Holland SD, Ramer LM, McMahon SB, Denk F, Ramer MS (2019) An ATF3-creert2 knock-in mouse for axotomy-induced genetic editing: proof of principle. eNeuro 6:2. 10.1523/eneuro.0025-19.2019

Kahle KT, Khanna A, Clapham DE, Woolf CJ (2014) Therapeutic restoration of spinal inhibition via druggable enhancement of potassium-chloride cotransporter KCC2-mediated chloride extrusion in peripheral neuropathic pain. JAMA Neurol 71:640–645. 10.1001/jamaneurol.2014.21 [PubMed: 24615367]

Kaila K, Price TJ, Payne JA, Puskarjov M, Voipio J (2014) Cation-chloride cotransporters in neuronal development, plasticity and disease. Nat Rev Neurosci 15:637–654. 10.1038/nrn3819 [PubMed: 25234263]

Kim J, Kobayashi S, Shimizu-Okabe C, Okabe A, Moon C, Shin T, Takayama CJ (2018) Changes in the expression and localization of signaling molecules in mouse facial motor neurons during regeneration of facial nerves. Chem Neuroanat 88:13–21. 10.1016/j.jchemneu.2017.11.002

Lee HH, Deeb TZ, Walker JA, Davies PA, Moss SJ (2011) NMDA receptor activity downregulates KCC2 resulting in depolarizing GABAA receptor-mediated currents. Nat Neurosci 14:736–743. 10.1038/nn.2806 [PubMed: 21532577]

Lee-Hotta S, Uchiyama Y, Kametaka S (2019) Role of the BDNF-TrkB pathway in KCC2 regulation and rehabilitation following neuronal injury: a mini review. Neurochem Int 128:32–38 [PubMed: 30986502]

Lorenzo LE, Godin AG, Ferrini F, Bachand K, Plasencia-Fernandez I, Labrecque S, Girard AA, Boudreau D, Kianicka I, Gagnon M, Doyon N, Ribeiro-da-Silva A, De Koninck Y (2020) Enhancing neuronal chloride extrusion rescues α2/α3 GABAA-mediated analgesia in neuropathic pain. Nat Commun 11:869. 10.1038/s41467-019-14154-6 [PubMed: 32054836]

Ludwig A, Uvarov P, Soni S, Thomas-Crusells J, Airaksinen MS, Rivera CJ (2011) Early growth response 4 mediates BDNF induction of potassium chloride cotransporter 2 transcription. J Neurosci 31:644–649. 10.1523/jneurosci.2006-10.2011 [PubMed: 21228173]

Markkanen M, Karhunen T, Llano O, Ludwig A, Rivera C, Uvarov P, Airaksinen MS (2014) Distribution of neuronal KCC2a and KCC2b isoforms in mouse CNS. J Comp Neurol 522:1897–1914. 10.1002/cne.23510 [PubMed: 24639001]

Medina I, Friedel P, Rivera C, Kahle KT, Kourdougli N, Uvarov P, Pellegrino C (2014) Current view on the functional regulation of the neuronal K(+)-Cl(−) cotransporter KCC2. Front Cell Neurosci 8:27. 10.3389/fncel.2014.00027 [PubMed: 24567703]

Miletic G, Miletic V (2008) Loose ligation of the sciatic nerve is associated with TrkB receptor-dependent decreases in KCC2 protein levels in the ipsilateral spinal dorsal horn. Pain 137:532–539. 10.1016/j.pain.2007.10.016 [PubMed: 18063479]

Moore YE, Deeb TZ, Chadchankar H, Brandon NJ, Moss SJ (2018) Potentiating KCC2 activity is sufficient to limit the onset and severity of seizures. Proc Natl Acad Sci USA 115:10166–10171. 10.1073/pnas.1810134115 [PubMed: 30224498]

Morado-Díaz CJ, Matarredona ER, Morcuende S, Talaverón R, Davis-López de Carrizosa MA, de la Cruz RR, Pastor AM (2014) Neural progenitor cell implants in the lesioned medial longitudinal fascicle of adult cats regulate synaptic composition and firing properties of abducens internuclear neurons. J Neurosci 34:7007–7017. 10.1523/jneurosci.4231-13.2014 [PubMed: 24828653]

Nabekura J, Ueno T, Okabe A, Furuta A, Iwaki T, Shimizu-Okabe C, Fukuda A, Akaike N (2002) Reduction of KCC2 expression and GABAA receptor-mediated excitation after in vivo axonal injury. J Neurosci 22:4412–4417. 10.1523/jneurosci.22-11-04412.2002 [PubMed: 12040048]

Oosthuyse B, Moons L, Storkebaum E et al. (2001) Deletion of the hypoxia-response element in the vascular endothelial growth factor promoter causes motor neuron degeneration. Nat Genet 28:131–138. 10.1038/88842 [PubMed: 11381259]

Palma E, Amici M, Sobrero F, Spinelli G, Di Angelantonio S, Ragozzino D, Mascia A, Scoppetta C, Esposito V, Miledi R, Eusebi F (2006) Anomalous levels of Cl− transporters in the hippocampal subiculum from temporal lobe epilepsy patients make GABA excitatory. Proc Natl Acad Sci USA 103:8465–8468. 10.1073/pnas.0602979103 [PubMed: 16709666]

Papp E, Rivera C, Kaila K, Freund TF (2008) Relationship between neuronal vulnerability and potassium-chloride cotransporter 2 immunoreactivity in hippocampus following transient forebrain ischemia. Neuroscience 154:677–689. 10.1016/j.neuroscience.2008.03.072 [PubMed: 18472345]

Patodia S, Raivich G (2012) Role of transcription factors in peripheral nerve regeneration. Front Mol Neurosci 5:8. 10.3389/fnmol.2012.00008 [PubMed: 22363260]

Payne JA, Stevenson TJ, Donaldson LF (1996) Molecular characterization of a putative K-Cl cotransporter in rat brain. A neuronal-specific isoform. J Biol Chem 271:16245–16252. 10.1074/jbc.271.27.16245 [PubMed: 8663311]

Payne JA, Rivera C, Voipio J, Kaila K (2003) Cation-chloride cotransporters in neuronal communication, development and trauma. Trends Neurosci 26:199–206. 10.1016/s0166-2236(03)00068-7 [PubMed: 12689771]

Peerboom C, Wierenga CJ (2021) The postnatal GABA shift: a developmental perspective. Neurosci Biobehav Rev 124:179–192. 10.1016/j.neubiorev.2021.01.024 [PubMed: 33549742]

Pozzi D, Rasile M, Corradini I, Matteoli M (2020) Environmental regulation of the chloride transporter KCC2: switching inflammation off to switch the GABA on? Transl Psychiatry 10:349. 10.1038/s41398-020-01027-6 [PubMed: 33060559]

Rivera C, Voipio J, Payne JA, Ruusuvuori E, Lahtinen H, Lamsa K, Pirvola U, Saarma M, Kaila K (1999) The K+/Cl− co-transporter KCC2 renders GABA hyperpolarizing during neuronal maturation. Nature 397:251–255. 10.1038/16697 [PubMed: 9930699]

Rivera C, Li H, Thomas-Crusells J, Lahtinen H, Viitanen T, Nanobashvili A, Kokaia Z, Airaksinen MS, Voipio J, Kaila K, Saarma M (2002) BDNF-induced TrkB activation down-regulates the K+-Cl− cotransporter KCC2 and impairs neuronal Cl− extrusion. J Cell Biol 159:747–752. 10.1083/jcb.200209011 [PubMed: 12473684]

Rivera C, Voipio J, Thomas-Crusells J, Li H, Emri Z, Sipilä S, Payne JA, Minichiello L, Saarma M, Kaila K (2004) Mechanism of activity-dependent downregulation of the neuron-specific K-Cl cotransporter KCC2. J Neurosci 24:4683–4691. 10.1523/jneurosci.5265-03.2004 [PubMed: 15140939]

Seijffers R, Mills CD, Woolf CJ (2007) ATF3 increases the intrinsic growth state of DRG neurons to enhance peripheral nerve regeneration. J Neurosci 27:7911–7920. 10.1523/jneurosci.5313-06.2007 [PubMed: 17652582]

Silva-Hucha S, Carrero-Rojas G, Fernández de Sevilla ME, Benítez-Temiño B, Davis-López de Carrizosa MA, Pastor AM, Morcuende S (2020) Sources and lesion-induced changes of VEGF expression in brainstem motoneurons. Brain Struct Funct 225:1033–1053. 10.1007/s00429-020-02057-y [PubMed: 32189115]

Talaverón R, Matarredona ER, de la Cruz RR, Pastor AM (2013) Neural progenitor cell implants modulate vascular endothelial growth factor and brain-derived neurotrophic factor expression in rat axotomized neurons. PLoS ONE 8:e54519. 10.1371/journal.pone.0054519 [PubMed: 23349916]

Tatetsu M, Kim J, Kina S, Sunakawa H, Takayama C (2012) GABA/glycine signaling during degeneration and regeneration of mouse hypoglossal nerves. Brain Res 1446:22–33. 10.1016/j.brainres.2012.01.048 [PubMed: 22325090]

Tovar-y-Romo LB, Zepeda A, Tapia R (2007) Vascular endothelial growth factor prevents paralysis and motoneuron death in a rat model of excitotoxic spinal cord neurodegeneration. J Neuropathol Exp Neurol 66:913–922. 10.1097/nen.0b013e3181567c16 [PubMed: 17917585]

Toyoda H, Ohno K, Yamada J, Ikeda M, Okabe A, Sato K, Hashimoto K, Fukuda A (2003) Induction of NMDA and GABAA receptor-mediated Ca2+ oscillations with KCC2 mRNA downregulation in injured facial motoneurons. J Neurophysiol 89:1353–1362. 10.1152/jn.00721.2002 [PubMed: 12612004]

Tsujino H, Kondo E, Fukuoka T, Dai Y, Tokunaga A, Miki K, Yonenobu K, Ochi T, Noguchi K (2000) Activating transcription factor 3 (ATF3) induction by axotomy in sensory and motoneurons: a novel neuronal marker of nerve injury. Mol Cell Neurosci 15:170–182. 10.1006/mcne.1999.0814 [PubMed: 10673325]

Uvarov P, Ludwig A, Markkanen M, Pruunsild P, Kaila K, Delpire E, Timmusk T, Rivera C, Airaksinen MS (2007) A novel N-terminal isoform of the neuron-specific K-Cl cotransporter KCC2. J Biol Chem 282:30570–30576. 10.1074/jbc.m705095200 [PubMed: 17715129]

Woo N-S, Lu J, England R, McClellan R, Dufour S, Mount DB, Deutch AY, Lovinger DM, Delpire E (2002) Hyperexcitability and epilepsy associated with disruption of the mouse neuronal-specific K-Cl cotransporter gene. Hippocampus 12:258–268. 10.1002/hipo.10014 [PubMed: 12000122]

Zacchigna S, Lambrechts D, Carmeliet P (2008) Neurovascular signaling defects in neurodegeneration. Nat Rev Neurosci 9:169–181. 10.1038/nrn2336 [PubMed: 18253131]

Zhu L, Polley N, Mathews GC, Delpire E (2008) NKCC1 and KCC2 prevent hyperexcitability in the mouse hippocampus. Epilepsy Res 79:201–212. 10.1016/j.eplepsyres.2008.02.005 [PubMed: 18394864]

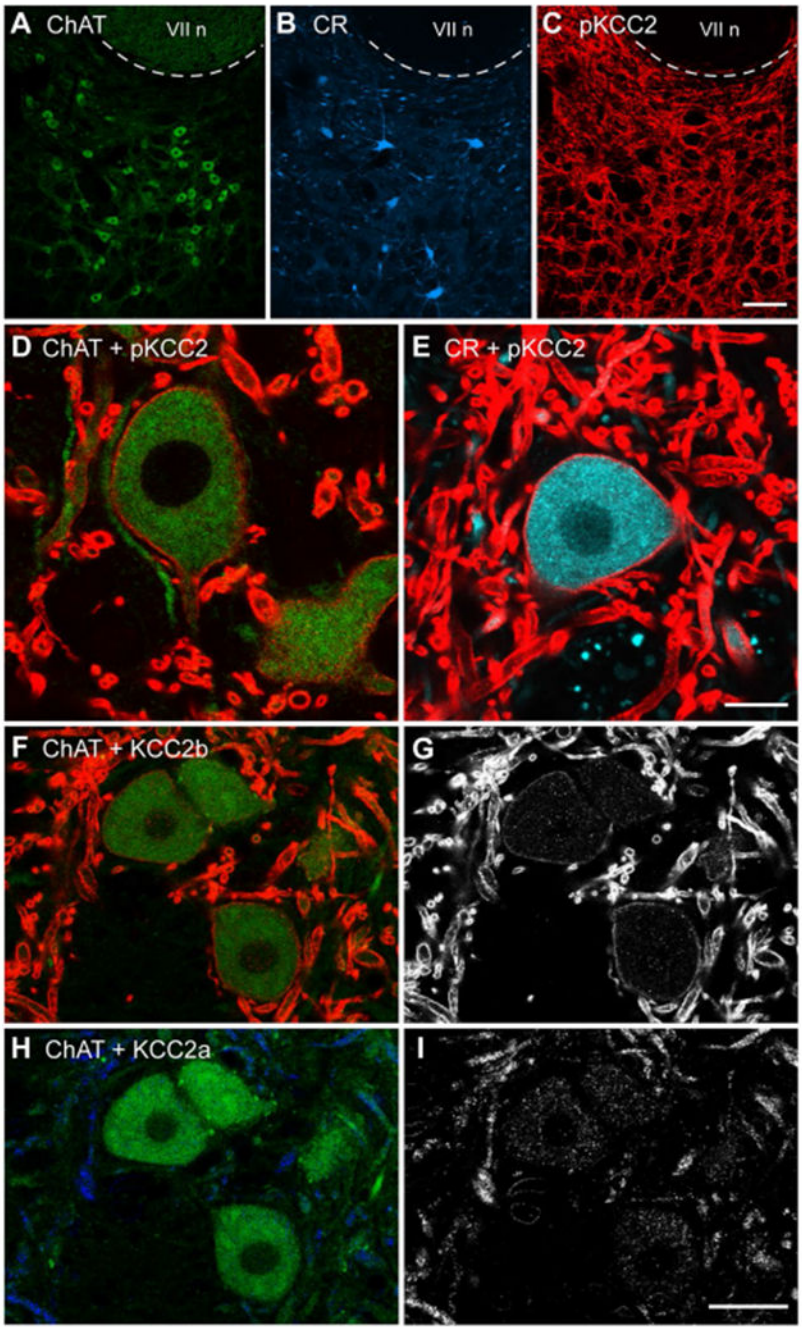

Fig. 1.

Presence of KCC2 and KCC2 isoforms in the cat abducens nucleus. **A–C** Low magnification confocal images (2D projection of a 50 μm confocal stack) of the abducens nucleus showing motoneurons labeled with choline acetyltransferase (ChAT) (**A**, green), abducens internuclear neurons labeled with calretinin (CR) (**B**, cyan) and pan-KCC2 (pKCC2 **C**, red) (dashed line delimits the facial nerve genu for anatomical orientation). **D** High magnification single plane confocal image showing double immunofluorescence for ChAT and pKCC2 in abducens motoneurons. **E** Same as **D** for an abducens internuclear neuron. **F–I** Single

plane confocal images showing triple immunofluorescence against ChAT (green in **F** and **H**), KCC2b (red in **F**) and KCC2a (blue in **H**) in abducens motoneurons. KCC2b and KCC2a are shown in black and white for better discrimination in **G** and **I.** KCC2b labeling of somata and dendrites is similar to pKCC2. KCC2a labeling was intracellular. Scale bars = 150 μm in *C* for **A–C**; 15 μm in **E** for **D–E**; 30 μm in ***I*** for **F–I**

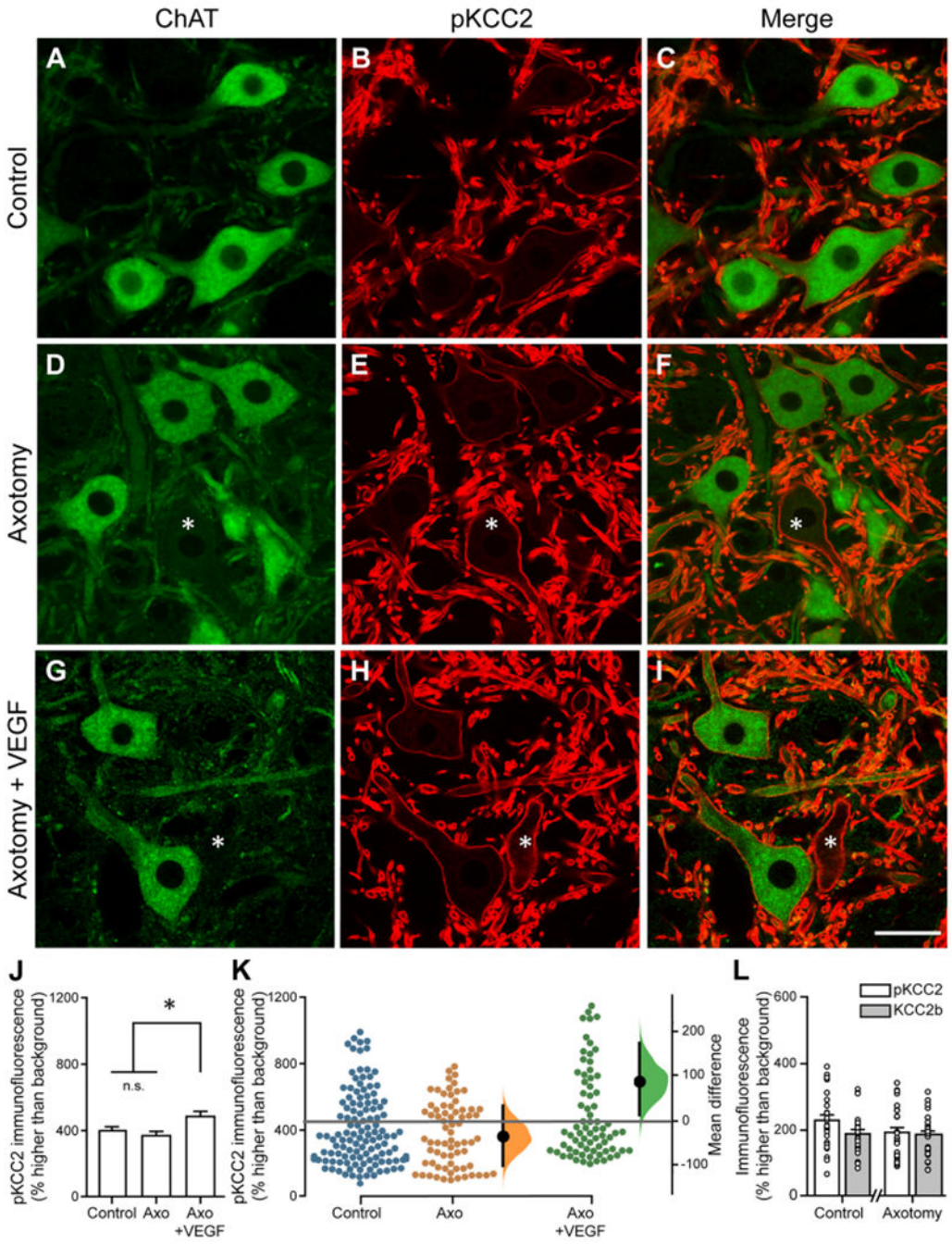

Fig. 2.

Changes in KCC2 levels induced by axotomy and VEGF administration in cat abducens motoneurons. **A, D, G** Confocal images showing abducens motoneurons identified by ChAT immunolabeling in the three experimental situations: control (**A**), axotomy (**D**), and axotomy plus VEGF administration (**G**). **B, E, H** Same regions as in **A, D** and **G,** respectively, but showing the red channel with pan(p)KCC2 immunostaining. **C, F, I** Merge of ChAT and pKCC2 immunolabelings. KCC2 immunolabels the surface of cell bodies and proximal dendrites of all motoneurons independent of the experimental condition. Asterisks in **D–I**

point to ChAT-immunonegative abducens internuclear neurons. **J** Quantitative comparison of pKCC2 immunofluorescence in abducens motoneurons in control, axotomy and axotomy + VEGF. No significant (n.s.) differences were observed between control and axotomized abducens motoneurons, whereas axotomized motoneurons treated with VEGF showed a significantly (asterisk) higher pKCC2 level than control ($p = 0.017$) and axotomized ($p = 0.004$) motoneurons, respectively; one-way ANOVA test followed by Holm-Sidak method; $n = 122$, 71 and 72 motoneurons analyzed in control, axotomized and axotomized + VEGF-treated conditions, respectively. **K** Swarm dot plots of raw data (individual motoneurons) and differences for comparisons against the shared control shown in Cumming estimation plots. The distribution of differences obtained from bootstrap resampling are shown with the mean difference depicted as a dot and the 95% confidence interval indicated by the ends of the vertical error bars. No statistically significant difference was found when comparing axotomy to control, but a 21% significant increase was detected in motoneurons treated with VEGF (two-sided permutation *t*-test $p = 0.0216$). **L** Quantitative analyses of pKCC2 and KCC2b in abducens motoneurons in control and axotomy. No significant differences (two-way ANOVA) were found according to the type of KCC2 immunoreactivity (pKCC2 or KCC2b; $p = 0.089$) or experimental condition (control or axotomized; $p = 0.166$). Scale bar = 40 μm in **I** for **A-I**

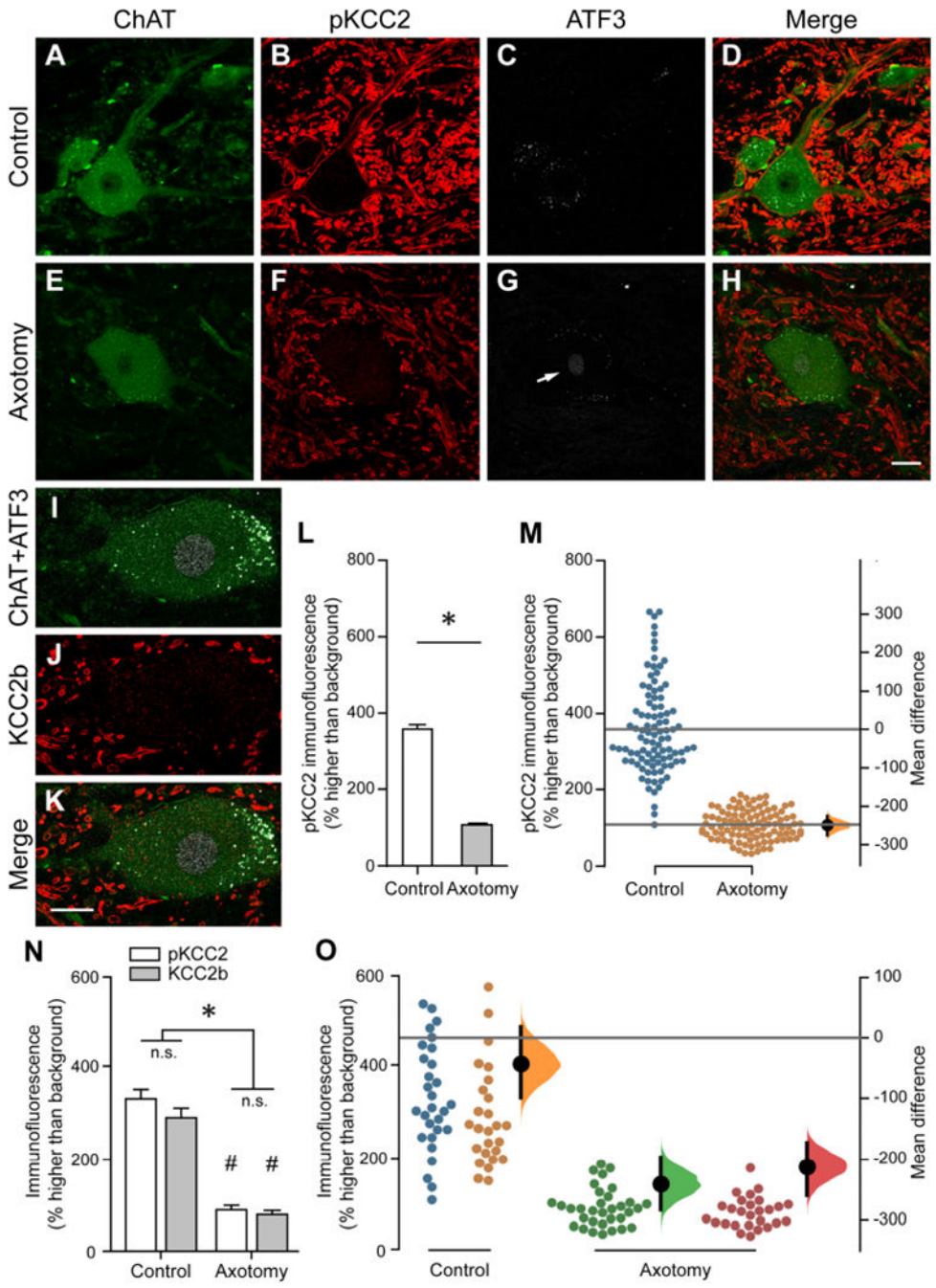

Fig. 3.

KCC2 changes induced by axotomy in cat spinal motoneurons. **A–H** High magnification single plane confocal images of spinal motoneurons immunostained against ChAT, pKCC2 and ATF3. **A–D** corresponds to a control motoneuron and **E–H** to a motoneuron axotomized 21 days previously. Individual immunoreactivities are presented in isolation and then merged (**D, H**), as indicated in the figure. Axotomized motoneurons expressed ATF3 in the nucleus (arrow in **G**) and decreased ChAT immunoreactivity (**E**). They also lacked surface pKCC2 immunoreactivity in the cell body and proximal dendrite surfaces (**F**). **I** Axotomized spinal

motoneuron immunolabeled for ChAT and ATF3. **J** KCC2b immunofluorescence of the same axotomized motoneuron as in **I** illustrating lack of KCC2b labeling in its somatic membrane. **K** Merge image of **I** and **J**. **L** Comparison of pKCC2 immunofluorescence between control and axotomized spinal motoneurons. Axotomized spinal motoneurons showed a significantly (asterisk) lower level of pKCC2 than control spinal motoneurons (*t*-test, $p \leq 0.001$; $n = 96$ and 101 control and axotomized motoneurons, respectively). **M** Swarm dot plots of raw data (individual motoneurons) and differences between control (blue) and axotomy (yellow) shown in Cumming estimation plots. The distribution of differences obtained from bootstrap resampling are shown with the mean difference depicted as a dot and the 95% confidence interval indicated by the ends of the vertical error bars. A 70% significant decrease was detected in axotomized spinal motoneurons (two-sided permutation *t*-test $p < 0.001$). **N** Bar chat illustrating the results of a two-way ANOVA test and Holm-Sidak method comparing the following two factors: experimental condition (control versus axotomy) and type of KCC2 immunoreactivity (pKCC versus KCC2b). Data were gathered from one cat stained in serial sections with pKCC2 and KCC2b (control, $n = 29$ and 26 motoneurons; axotomy, $n = 33$ and 27 motoneurons for pKCC2 and KCC2b, respectively). Two-way ANOVA detected significant differences in control vs. axotomized motoneurons (asterisk, $p < 0.001$), but no difference between pKCC2 and KCC2b ($p = 0.099$, *n.s.*), or the interaction between axotomy and type of immunoreactivity ($p = 0.334$). Post hoc Holm-Sidak pairwise comparisons revealed significant difference between control and injured motoneuron for pKCC2 and KCC2b (#, $p < 0.001$ for both). **O** Swarm dot plots of raw data (individual motoneurons) and differences between pKCC2 in control (blue), KCC2b in control (yellow) and pKCC2 after axotomy (green) and KCC2b after axotomy (red) all shown in Cumming estimation plots. The distribution of differences obtained from bootstrap resampling are shown with the mean difference depicted as a dot and the 95% confidence interval indicated by the ends of the vertical error bars. No significant differences were found between KCC2b and pKCC2 in control motoneurons. Axotomized motoneurons showed a 70% significant decrease compared to their respective antibody matched controls (two-sided permutation *t*-test $p < 0.001$ in both comparisons). Scale bars = 30 μm in **H** for **A–H**; 20 μm in **K** for **I–K**

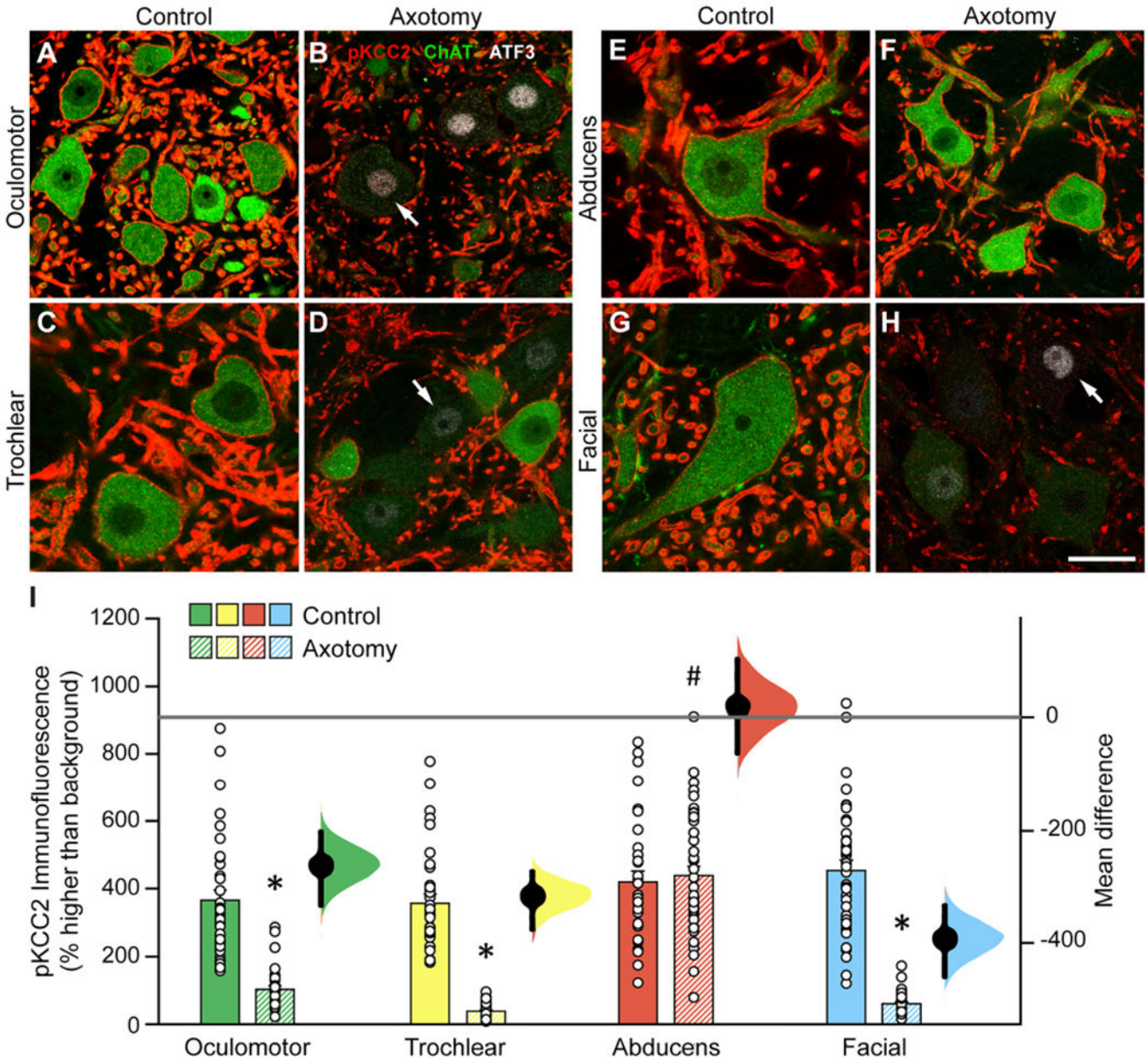

Fig. 4.

KCC2 immunoreactivity in brainstem oculomotor, trochlear, abducens and facial motoneurons, in control and after axotomy, in the rat. **A, C, E, G** Confocal images of double immunofluorescence against ChAT (green) and pKCC2 (red) in control oculomotor (**A**), trochlear (**C**), abducens (**E**) and facial (**G**) motoneurons. **B, D, F, H** Confocal images of triple immunofluorescence against ChAT (green), KCC2 (red) and ATF3 (white) in the same brainstem nuclei, but after axotomy. Axotomized oculomotor, trochlear and facial motoneurons showed a marked reduction in pKCC2 and ChAT. ATF3 is a general marker of axotomized motoneurons and labels the cell nucleus, as can be observed in axotomized oculomotor (**B**), trochlear (**D**) and facial (**H**) motoneurons (some examples are indicated by white arrows). However, in axotomized abducens motoneurons (**F**), immunostaining

for pKCC2 and ChAT showed a similar appearance to control (**E**), and ATF3 labeling was absent. **I** Quantification of KCC2 immunofluorescence in the four nuclei (oculomotor, trochlear, abducens and facial) and in the control and axotomy situation. Asterisks indicate significant ($p < 0.001$) difference between control and axotomized motoneurons within the same nucleus. Hashtag indicates significant difference ($p < 0.001$) between axotomized abducens motoneurons and the axotomized motoneurons of the other three nuclei (Two-way ANOVA followed by Holm-Sidak method; $n = 35$, 36, 33 and 39 for control and $n =$ 33, 35, 44 and 42 for axotomized motoneurons of the oculomotor, trochlear, abducens and facial nuclei, respectively). Data in histograms represent mean ± SEM. Depicted to the right are the Cumming plots of estimated differences after bootstrap resampling with average difference indicated by a dot and 95% CI limit of the distribution by the vertical bars. Oculomotor, trochlear and facial motoneurons all showed significant reduction of 72%, 89% and 87% of the control value, respectively (two-sided permutation *t*-test $p < 0.001$ for all comparisons). There were no significant differences when comparing axotomized and control motoneurons in the abducens nucleus. Scale bar = 30 μm in **H** for **A–H**

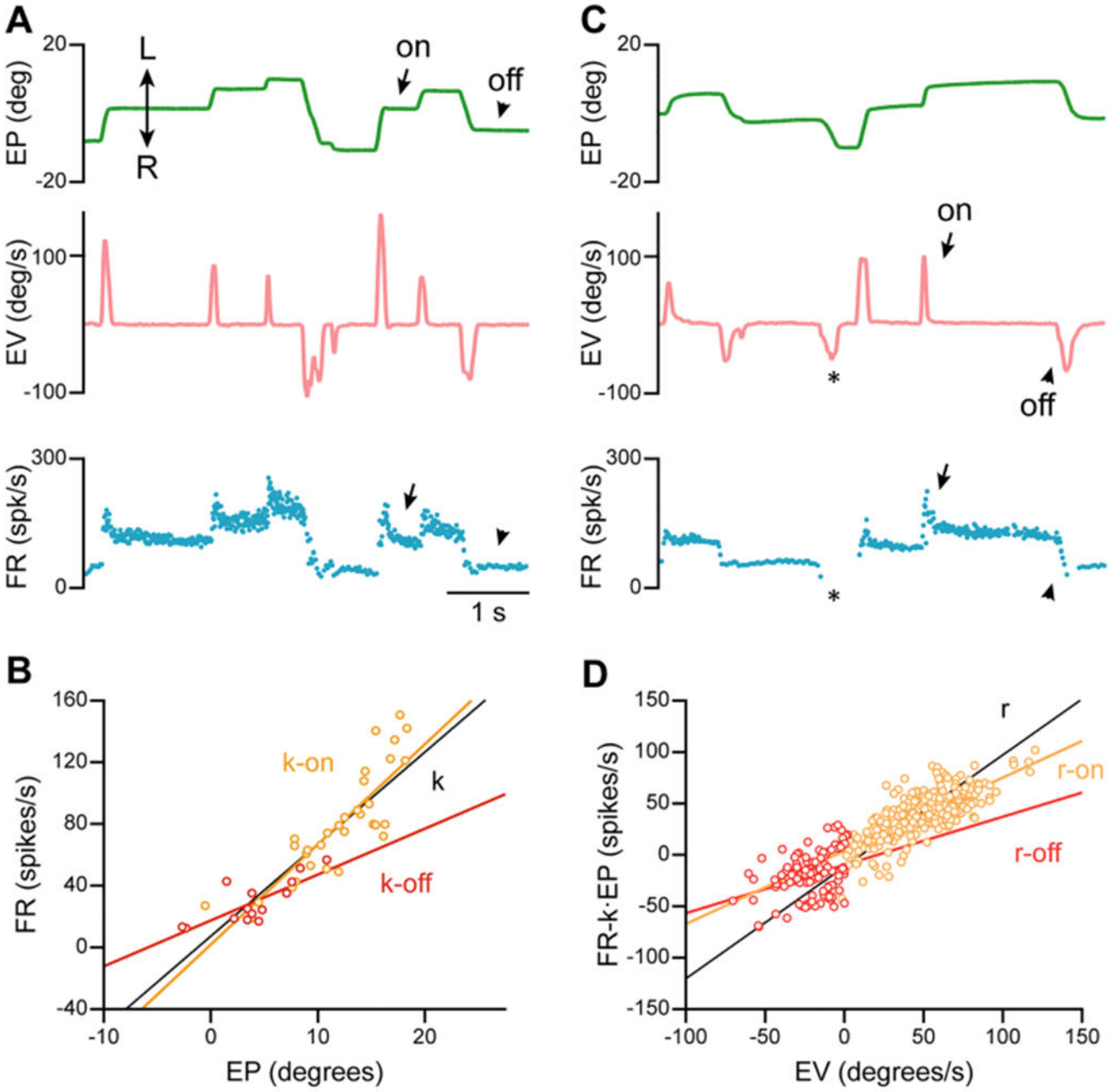

Fig. 5.

Procedure to calculate k-on, k-off, r-on and r-off in the discharge activity of abducens motoneurons. In **A** and **C**, from top to bottom: eye position (EP, in degrees), eye velocity (EV, in degrees/s) and firing rate (FR, in spikes/s) of a control abducens motoneuron during spontaneous eye movements. The double arrow in **A** indicates leftward (L) and rightward (R) eye movements. **B** FR and EP correlates by means of a linear regression line whose slope represents the neuronal eye position sensitivity (k, in spikes/s/degree; line in black). When eye fixations are separated between those occurring after an on-directed saccade (arrows in **A** in the traces of EP and FR) and those after an off-directed saccade (arrowheads

in **A** in the traces of EP and FR), then the neuronal eye position sensitivity can be calculated independently for on-fixations versus off-fixations, thus obtaining the parameters k-on (in orange) and k-off (in red), respectively. **D** The neuronal eye velocity sensitivity during saccades (r, in spikes/s/ degree/s) is obtained as the slope of the linear regression line between FR (previous subtraction of the EP component, FR-k·EP) and EV (line in black). If the analysis is performed separating on-directed saccades and their corresponding neuronal bursts in FR (arrows in **C** in the traces of EV and FR) from off-directed saccades and their corresponding decreases in FR (arrowheads in **C** in the traces of EV and FR), then r-on (in orange) and r-off (in red) sensitivities, respectively, are obtained. Off-directed saccades accompanied by a cut-off in FR (asterisks in **C**) were discarded from the calculation of r-off parameter

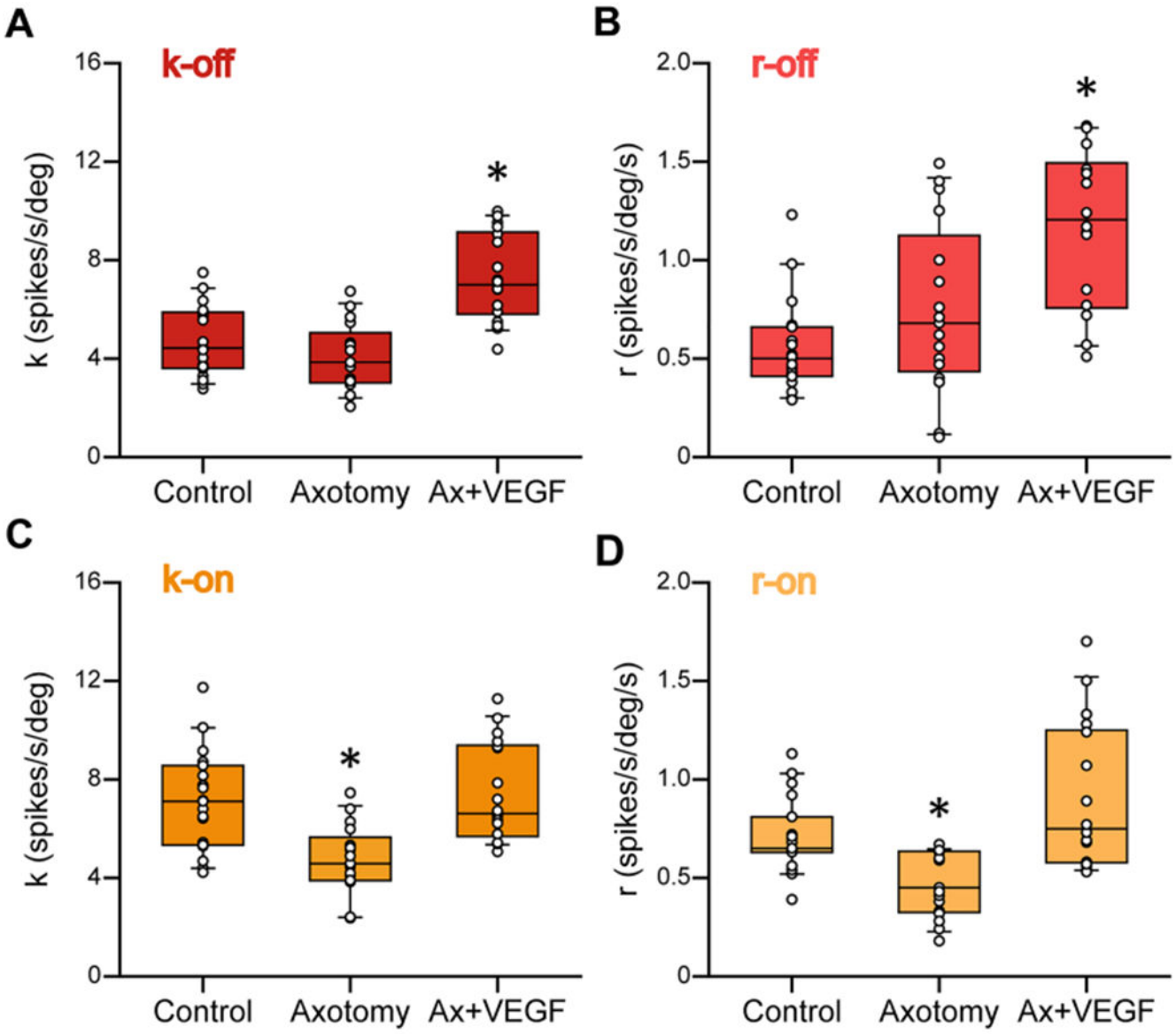

Fig. 6.

Quantitative analysis of neuronal sensitivities to eye position and velocity depending on the on- or off-direction of the fixation or saccade. **A, B** Plots representing neuronal eye position sensitivity during off-fixations (k-off, in **A**) and neuronal eye velocity during off-saccades (r-off, in **B**) illustrated for the three experimental groups: control, axotomy, and axotomy + VEGF. **C, D** Same as **A, B** but for k-on (**C**) and r-on (**D**). The asterisks in **A, B** indicate significant difference ($p < 0.05$) in k-off (**A**) and r-off (**B**) between the axotomized motoneurons treated with VEGF with respect to control and axotomized untreated motoneurons. In **C, D** the asterisks indicate significant differences ($p < 0.05$) between axotomy versus the other two groups (for **A–D**, one-way ANOVA test, $p \leq 0.001$, followed by Dunn's method for all pairwise multiple comparisons). The number

of motoneurons analyzed in control, axotomy and axotomy + VEGF was 21, 17 and 18, respectively

Table 1

Animals used in this study

Animal #	Surgery	Treatment	Survival (days)	Chronic recordings
Cat 1–4	Left VIth nerve cut	Axotomy + VEGF	20 + 20	Yes
Cat 5–6	Left VIth nerve cut	Axotomy + VEGF	20 + 20	No
Cat 7–9	Left VIth nerve cut	Axotomy	20–21	No
Cat 10–12	Left tibial nerve cut	Axotomy	21	No
Rat 1–3	Left eye enucleation and facial nerve cut	Axotomy	15	No

Table 2

Antibodies used in this study

Antigen	Immunogen	Host/type	Manufacturer	RRID and Specificity	Dilution
Pan KCC2	N-terminal His-tag fusion protein of rat KCC2 aa 932-1043	Rabbit/polyclonal	Millipore Cat #07–432	AB_310611 and AB_11213615	1:500
KCC2a	Mouse KCC2a N-terminus aa 20–40	Rabbit/polyclonal	Dr M Airaksinen, University of Helsinki, Finland	RRID NA Tested against KCC2a KO[1]	1:250
KCC2b	Mouse KCC2b N-terminus aa 8–22	Chicken/polyclonal	Dr M Airaksinen, University of Helsinki, Finland	RRID NA Tested by comparison of KCC2 null and KCC2a KOs[1]	1:750
ChAT Used for cell type identification	Human placental enzyme	Goat/polyclonal	Millipore Cat #AB144P	AB_2079751 Identities Chat expressing motoneurons in Chat-Cre mice	1:500
Calretinin Used for cell type identification	Recombinant human calretinin-22 k	Mouse/monoclonal	Swant Clone 6B3	AB_10000320 Recognizes an epitope within the first 4 EF-hands domains common to both calretinin and calretinin-22k[2] Identifies abducens interneurons[3]	1:100
ATF3 Used for injured motoneuron identification	Recombinant protein corresponding to aa 1-103 in human ATF3	Mouse/monoclonal	Novus Clone 1685 NBP2-34489	AB_2786997 Recognizes the epitope: ASAIVPCLSPPGSL (Manufacturer's information) Not present in uninjured motoneurons	1:200